Elucidating the Origin of Anomalous Diffusion in Crowded Fluids

Jedrzej Szymanski and Matthias Weiss

Cellular Biophysics Group (BIOMS), German Cancer Research Center, Im Neuenheimer Feld 280, D-69120 Heidelberg, Germany

(Received 12 December 2008; published 15 July 2009)

Anomalous diffusion in crowded fluids, e.g., in the cytoplasm of living cells, is a frequent phenomenon. So far, however, the associated stochastic process, i.e., the propagator of the random walk, has not been uncovered. Here we show by means of fluorescence correlation spectroscopy and simulations that the properties of crowding-induced subdiffusion are consistent with the predictions for fractional Brownian motion or obstructed (percolationlike) diffusion, both of which have stationary increments. In contrast, our experimental results cannot be explained by a continuous time random walk with its distinct non-Gaussian propagator.

DOI: 10.1103/PhysRevLett.103.038102 PACS numbers: 87.15.Vv, 05.40.Fb, 87.10.Mn, 87.80.Nj

Crowded fluids are a natural phenomenon in living cells with considerable impact on intracellular chemical reactions (see, e.g., [1] for a review). Indeed, the cytoplasm and nucleoplasm of living cells are crowded with a plethora of macromolecules, often rendering the diffusion in these intracellular fluids anomalous [2–5]. While the interior of cells is very complex and heterogenous, the phenomenon of crowding-induced subdiffusion has also been observed in more controlled *in vitro* approaches, for example, in entangled actin networks [6] and concentrated protein solutions [3,7,8]. In all of these cases, a nonlinear growth of the mean square displacement (MSD) $\langle r(t)^2 \rangle \sim t^\alpha$ with $\alpha < 1$ has been observed.

Despite the frequent observation of a nonlinear growth of the MSD in crowded media (see [9] for examples where normal diffusion has been reported), the properties of the associated propagator have remained elusive so far. Indeed, one may group the propagators for subdiffusive motion into two categories: those that are associated with stationary increments and those that arise from nonstationary increments. Prominent examples of the first category are fractional Brownian motion (FBM), for which the propagator reads $P(r, t) \sim \exp\{-Cr^2/t^{(2\alpha-1)/2}\}/t^{(2\alpha-1)/2}$ [10], and percolation with $P(r, t) \sim y \exp\{-Cy^{1.65}\}$, $y = r/t^{\alpha/2}$ [11,12]. The most prominent nonstationary process is a continuous time random walk (CTRW) with its distinct non-Gaussian propagator [Eq. (42) in [13]]. Indeed, due to the intrinsic aging process, a CTRW shows weak ergodicity breaking; i.e., in strong contrast to FBM and obstructed (percolationlike) diffusion, the time and ensemble averages of the MSD do not coincide for a CTRW [14,15].

Here we have utilized fluorescence correlation spectroscopy (FCS) to elucidate the propagator underlying crowding-induced subdiffusion. In particular, we have quantified the anomaly α and the mean residence time τ_D in the focus for apoferritin in crowded dextran solutions. Comparing the obtained distributions $p(\alpha)$ and $p(\tau_D)$ with simulation results on FBM, obstructed diffusion, and CTRW, we find a good agreement with the first two yet strong deviations from the predictions of a CTRW. Our data hence indicate that it is a stochastic process with stationary increments that is more appropriate for describing crowding-induced subdiffusion.

Materials and methods.—FCS curves were acquired using a MicroTime 200 microscope (Picoquant) equipped with a $60x/1.2$ NA water immersion objective. As a fluorescent probe we labeled apoferritin (Sigma) with Alexa488 (Molecular Probes) using the manufacturer's protocol. After purification, the labeled apoferritin was immersed in a crowded dextran solution (concentration: 20% by weight) using 500 kDa dextran (Sigma) as a crowding agent. The fluorophore was excited with a pulsed 470 nm laser that did not fully illuminate the back aperture plane; the width of the FCS focus was hence not diffraction-limited but had a slightly larger width ($r_0 \approx$ 320 nm).

FCS data were fitted with a versatile expression for subdiffusion in bulk solution [3]:

$$C(\tau) = \frac{1}{N[1 + (\tau/\tau_D)^\alpha]\sqrt{1 + q(\tau/\tau_D)^\alpha}}. \quad (1)$$

Here α denotes the anomaly degree of the diffusion, while τ_D is the mean residence time of a particle in the confocal volume [for $\alpha = 1$ the diffusion coefficient D is given via $\tau_D = r_0^2/(4D)$ with the beam waist r_0]. The mean number of particles in the confocal volume is denoted by N. The prefactor $q < 1$ denotes the unavoidable elongation of the confocal volume along the optical axis. In our case, $q \approx 1/36$. Fitting was performed with XMGRACE using the interval 100 μs $\leq \tau \leq$ 200 ms. Since the fitting range is well above the triplet decay time of Alexa488 (<5 μs) and as the anticipated triplet fraction also is very low, we have not included a triplet contribution into Eq. (1).

FCS data were acquired in phosphate buffered saline (PBS) or a crowded dextran solution by parking the laser beam in the solution and detecting the fluorescence for a period of 180 s. Without moving the beam or the fluid, this acquisition was repeated 50 times to gain statistics for α

and τ_D. In all measurements, the mean particle number in the focus was $1 < N < 10$.

Anomalous diffusion was simulated by (i) fractional Brownian motion, (ii) obstructed diffusion, and (iii) a CTRW. In case (i), we used the approach outlined in Ref. [16] and adjusted the generalized mobility, i.e., the value of the typical spatial increment taken within one simulation time unit, to match the experimentally observed residence time τ_D while α was fixed beforehand. For (ii) and (iii), we used a two-dimensional square lattice with periodic boundary conditions and the blind ant algorithm. A computationally inexpensive two-dimensional simulation indeed captures the dominant contribution to the autocorrelation decay in the range $\tau < 1$ s as the correlation decay in Eq. (1) is dominated by diffusion perpendicular to the optical axis [cf. factor $q \approx 1/36$ in Eq. (1)]. For obstructed diffusion, we randomly placed immobile obstacles on 35%–37% of the lattice sites. This obstacle density was chosen to yield a good match between the experimentally observed mean anomaly $\langle\alpha\rangle$ and the one derived from the ensemble-averaged MSD in the simulations. Tracer particles were assumed to have a diffusion constant $D = 1.6\ \mu\text{m}^2/\text{s}$. The lattice size was 350×350 with a lattice constant of $\Delta x = 10$ nm (in accordance with the free hydrodynamic radii of dextran, ≈ 6.5 nm [3], and apoferritin, ≈ 6 nm); the time increment was $\Delta t = 6.25\ \mu$s. For simulating a CTRW, we used the same lattice but chose a diffusion coefficient $D = 62.5\ \mu\text{m}^2/\text{s}$ and a time increment of $\Delta t = 0.1\ \mu$s. After having taken a diffusive step, particles were assigned a random waiting time $\tau = 1/\xi^{1/\alpha}$ with $0 < \xi < 1$ a uniform random number. The distribution of waiting times hence had a power-law tail $p(\tau) \sim 1/\tau^{1+\alpha}$, and the ensemble-averaged mean square displacement grew like $\langle r(t)^2\rangle \sim t^\alpha$ for $t > 1\ \mu$s. Choosing waiting times $\tau < \Delta t$ resulted in a normal diffusive behavior with the imposed diffusion coefficient.

To obtain FCS curves from the simulations, a Gaussian confocal volume of width $\sigma_x = \sigma_y = 250$ nm was placed in the center of the simulation box, and particles were assumed to contribute to the total fluorescence proportional to the value of the Gaussian beam profile on their lattice site. For consistency with the experiments, we used 300 particles in all simulations, yielding a mean particle number $1 < N < 10$ in the focus. To have the same statistics for α and τ_D as in the experiment, we started 50 independent simulations for each process (CTRW, obstructed diffusion, and FBM), yielding 50 simulated FCS curves. As we simulated only two-dimensional diffusion, we have set $q = 0$ in Eq. (1) when doing the fitting. Fitting in all cases was performed with XMGRACE using the interval $100\ \mu\text{s} \leq \tau_D \leq 200$ ms.

Results and discussion.—We first measured the diffusion of apoferritin in buffer solution (PBS). In all cases, we observed normal diffusion with a mean residence time $\langle\tau_D\rangle \approx 720\ \mu$s (Fig. 1). Apoferritin has an approximate radius of 6 nm, yielding a diffusion coefficient of about $38\ \mu\text{m}^2/\text{s}$ via the Einstein-Stokes equation (assuming that PBS has the viscosity of water, $\eta = 10^{-3}$ Pa s). This translates to a diffusion time $\tau_D = r_0^2/(4D) \approx 675\ \mu$s, when including the focus width $r_0 \approx 320$ nm. This theoretical estimate is in good agreement with the experimentally found value.

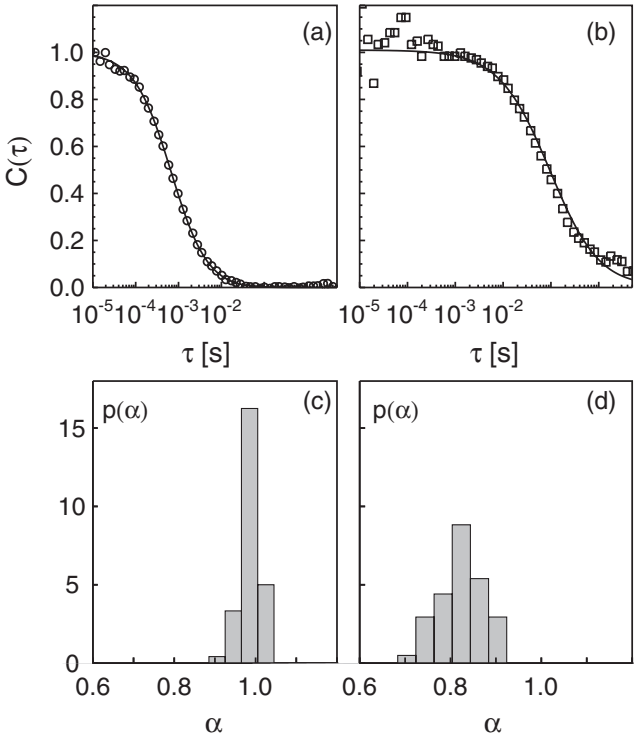

FIG. 1. Representative (normalized) FCS curve for apoferritin (a) in PBS ($\alpha = 1$, $\tau_D = 675\ \mu$s) and (b) in a crowded dextran solution ($\alpha = 0.81$, $\tau_D = 97.6$ ms). (c) The distribution of the anomaly $p(\alpha)$ in PBS is very narrow with a mean $\langle\alpha\rangle \approx 0.99$. (d) In a crowded dextran solution, a broadening of $p(\alpha)$ and a shift of the mean ($\langle\alpha\rangle \approx 0.82$) is clearly visible.

In contrast to the observations in PBS, the diffusion in crowded dextran solutions was strongly anomalous ($\langle\alpha\rangle \approx 0.82$) in agreement with previous reports [3,7]. Also, the anomaly degree varied more strongly than for measurements in PBS (Fig. 1). Moreover, we did not observe any systematic variation of α, e.g., due to aging of the sample, hence indicating that a CTRW may not be an adequate description for the stochastic process monitored in the FCS experiments. Extracting the complex shear modulus $G(\omega) = G'(\omega) + iG''(\omega)$ from the experimental FCS data (see [5] for details) showed that the crowded dextran solution did not exhibit properties of glasses or cross-linked gels [i.e., no plateau in $G(\omega)$] but rather was a viscoelastic fluid with $G'' > G'$. Previous work of ours also had shown that fluorescent dextran molecules in a fluid of nonfluorescent dextran crowders are quite mobile ($\tau_D < 100$ ms, depending on the actual crowding condi-

tions) [3]. This suggests a fluid rather than a gel-like nature of the crowded dextran solution.

To elucidate if FBM, CTRW, or obstructed diffusion could account for the observed distribution of anomalies, we performed simulations on these respective stochastic processes (see above for details). First, we inspected directly the diffusion paths of particles. As evidenced by the ensemble-averaged MSD, all simulations reproduced a subdiffusive motion with $\alpha = 0.82$ (Fig. 2). While the value of α had been imposed as a parameter in FBM and CTRW, the actual value of the anomaly for obstructed diffusion is imposed indirectly via choosing the obstacle density. As expected for obstructed diffusion below the percolation threshold, the MSD showed a transition towards normal diffusion for large times (here, $t > 1$ s). In agreement with the expectation of an ergodic behavior, the ensemble-averaged MSD and its time-averaged analogon (using a representative trajectory) coincided within the statistical error for obstructed diffusion and FBM. In contrast, for the CTRW only the ensemble-averaged MSD yielded subdiffusion in agreement with the imposed α value. The time-averaged MSD, however, showed normal diffusion. This behavior is anticipated and has been reported earlier as a consequence of the weak ergodicity breaking in a CTRW [14,15].

Having verified that the simulations yielded the anticipated scaling of the MSD, we next inspected the variability of the anomaly α for individual FCS simulation runs. For each simulated FCS curve, we fitted the correlation function with Eq. (1) and extracted α and τ_D. For FBM and obstructed diffusion (obstacle concentration 35%–37%), we found fairly narrow distributions that matched well the experimentally determined $p(\alpha)$ [Fig. 3(a)]. It is worthwhile noting that obstructed diffusion at a given concentration of obstacles (e.g., 36%) with random configurations of the obstacles yielded a more narrow distribution $p(\alpha)$. This indicates that a certain amount of (dynamic) variability in the obstacle configuration is necessary to describe the experimental data. For FBM we observed a mean anomaly $\langle\alpha\rangle \approx 0.84$ that was slightly higher than the value imposed in the simulations ($\alpha = 0.82$).

In contrast to FBM and obstructed diffusion, a CTRW with $\alpha = 0.82$ resulted in a very broad distribution of anomalies [Fig. 3(b)]. Also the mean of the distribution ($\langle\alpha\rangle \approx 0.59$) strongly deviates from the α value imposed in the waiting time statistics. This discrepancy is not observed in the ensemble-averaged MSD (cf. Fig. 2) and hence appears to be a consequence of the small amount of particles that contribute to the FCS curve at each instant of time. We also had confirmed earlier that Eq. (1) indeed can be used to fit $C(\tau)$ when particles move according to the fractional Fokker-Planck equation [3], i.e., the mean-field description of a CTRW. We had found that the use of Eq. (1) leads to a slight underestimation of the anomaly ($\alpha_{\mathrm{Eq.(1)}} = 1.1 * \alpha_{\mathrm{CTRW}} - 0.12$) yielding $\alpha_{\mathrm{Eq.(1)}} = 0.78$ for the imposed value $\alpha_{\mathrm{CTRW}} = 0.82$. Yet, the observed value $\langle\alpha\rangle \approx 0.59$ clearly is much smaller, and the anomaly distribution for a CTRW (as deduced from the simulated FCS

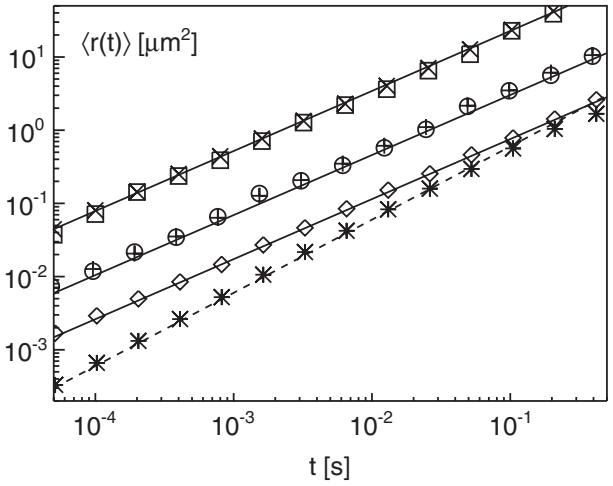

FIG. 2. Mean square displacement $\langle r(t)^2\rangle$ for obstructed diffusion (36% obstacle concentration), FBM, and CTRW (from top). Open symbols denote the ensemble-averaged MSD, and cross-like symbols denote the time-averaged MSD for a representative trajectory. While both approaches coincide for FBM and obstructed diffusion, the curves differ for the CTRW due to weak ergodicity breaking. For better visibility, MSD curves for FBM and obstructed diffusion have been shifted upwards (factor 50 and 250, respectively). Full lines scale as $\langle r(t)^2\rangle \sim t^{0.82}$; the dashed line is linear in time.

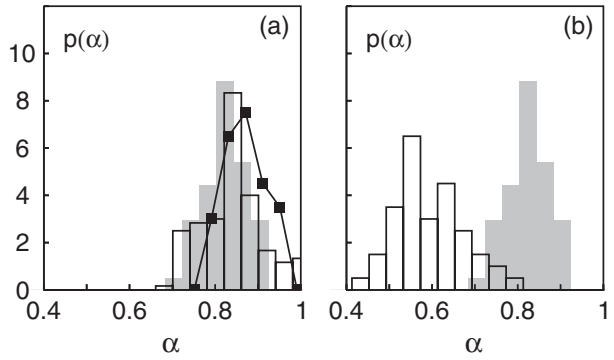

FIG. 3. (a) Distribution of the anomaly $p(\alpha)$ obtained for obstructed diffusion with 35%–37% obstacle density (black line histogram). The width of the distribution agrees well with the experimental data (gray-shaded histogram; cf. Fig. 1). Data for FBM are shown as filled squares connected by full lines. While here the width of the distribution is consistent with the experimental data, a slight shift in the mean anomaly ($\langle\alpha\rangle \approx 0.84$) with respect to the value imposed in the simulation ($\alpha = 0.82$) is observed. (b) The distribution obtained for a CTRW (black line histogram) yielded an average anomaly ($\langle\alpha\rangle \approx 0.59$) that was much lower than the value imposed in the waiting time statistics ($\alpha = 0.82$). Moreover, the CTRW-derived distribution is much broader than the experimental distribution (gray-shaded histogram).

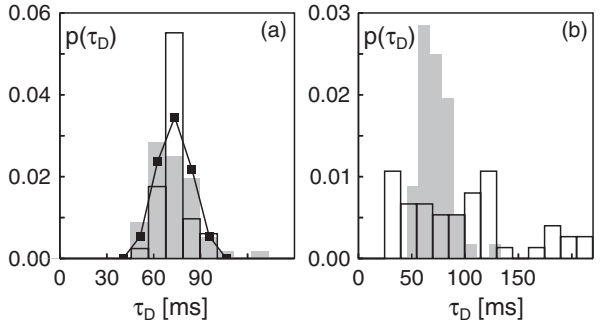

FIG. 4. (a) The distribution $p(\tau_D)$ of mean residence times in the confocal volume obtained for obstructed diffusion with 35%–37% obstacle density (black line histogram) is in very good agreement with the experimentally determined distribution (gray-shaded histogram). The distribution for FBM (filled squares connected by full lines) also agrees well with the experimental data. (b) The distribution of residence times obtained for a CTRW with $\alpha = 0.82$ (black line histogram) is shifted towards larger values and appears quite broad as compared to the experimental data (gray-shaded histogram).

curves) is therefore inconsistent with the experimental data [17].

As a second quantity, we inspected the distribution of residence times in the focus $p(\tau_D)$ that encodes the generalized mobility of the particles (i.e., the analogue to the diffusion coefficient with units $\mu m^2/s^\alpha$). Similar to our results on the distribution of anomalies, we find a good agreement of the experimental data and the simulations of FBM and obstructed diffusion [Fig. 4(a)]. In contrast, a CTRW produced larger residence times with a broader distribution than the experimentally determined $p(\tau_D)$ [Fig. 4(b)]. Thus, also the distribution of residence times supports the notion that crowding-induced subdiffusion is more consistent with FBM and obstructed diffusion than with a CTRW.

Having ruled out CTRW as a possible explanation for our experimental observations, one may ask whether it is also possible to discriminate between FBM and obstructed diffusion. We speculate that one may address this point by monitoring the variation of α as the concentration of the crowding agent is varied. The resulting experimental data can subsequently be checked for consistency with Monte Carlo simulations on FBM or obstructed diffusion with varying concentrations of obstacles [18]. Given that obstructed diffusion relies on (almost) immobile obstacles while our crowded solution rather is a fluid (i.e., obstacles move quite rapidly), it is tempting to speculate that these additional experiments and simulation will reveal that obstructed diffusion does not represent the most adequate stochastic process to describe crowding-induced subdiffusion.

In conclusion, crowding-induced subdiffusion is most consistent with a stochastic process that has stationary increments. By using a CTRW, a similar (ensemble-averaged) MSD is observed, yet due to the weak ergodicity breaking strong fluctuations in the anomaly and generalized mobility of single trajectories are expected [14,15] that are inconsistent with the experimentally observed distributions for $p(\alpha)$ and $p(\tau_D)$. It will be interesting to use single-particle tracking on crowded media to obtain a more direct discrimination among CTRW, FBM, and obstructed diffusion since time- and ensemble-averaged MSD can be calculated directly. In this context, also finite-size effects and restricted measurement times may be included that affect FBM [19] and CTRW [14].

This work was supported by the Institute for Modeling and Simulation in the Biosciences (BIOMS) in Heidelberg. J. S. received funding by the Initiative and Networking Fund of the Helmholtz Association within the Helmholtz Alliance on Systems Biology. We thank Picoquant for technical support.

[1] A. Minton, J. Cell Sci. **119**, 2863 (2006).
[2] I. Tolic-Nørrelykke, E. Munteanu, G. Thon, L. Oddershede, and K. Berg-Sørensen, Phys. Rev. Lett. **93**, 078102 (2004).
[3] M. Weiss, M. Elsner, F. Kartberg, and T. Nilsson, Biophys. J. **87**, 3518 (2004).
[4] I. Golding and E. Cox, Phys. Rev. Lett. **96**, 098102 (2006).
[5] G. Guigas, C. Kalla, and M. Weiss, Biophys. J. **93**, 316 (2007).
[6] I. Wong, M. Gardel, D. Reichman, E. Weeks, M. Valentine, A. Bausch, and D. Weitz, Phys. Rev. Lett. **92**, 178101 (2004).
[7] D. Banks and C. Fradin, Biophys. J. **89**, 2960 (2005).
[8] W. Pan, L. Filobelo, N. D. Q. Pham, O. Galkin, V. V. Uzunova, and P. G. Vekilov, Phys. Rev. Lett. **102**, 058101 (2009).
[9] J. A. Dix and A. S. Verkman, Annu. Rev. Biophys. **37**, 247 (2008).
[10] K. Sebastian, J. Phys. A **28**, 4305 (1995).
[11] S. Havlin and D. Ben-Avraham, Adv. Phys. **36**, 695 (1987).
[12] B. Yuste, J. Phys. A **28**, 7027 (1995).
[13] R. Metzler and J. Klafter, Phys. Rep. **339**, 1 (2000).
[14] Y. He, S. Burov, R. Metzler, and E. Barkai, Phys. Rev. Lett. **101**, 058101 (2008).
[15] A. Lubelski, I. M. Sokolov, and J. Klafter, Phys. Rev. Lett. **100**, 250602 (2008).
[16] G. Guigas and M. Weiss, Biophys. J. **94**, 90 (2008).
[17] We also tried fitting with a recently derived analytical expression for a CTRW [A. Lubelski and J. Klafter, Biophys. J. **96**, 2055 (2009)]. This fitting procedure, however, was very time-consuming and unstable since the analytical expression involves an infinite sum and an integral that can be reduced to a closed form only for $\alpha = 1/2, 1/3$.
[18] Such a study is currently in progress.
[19] W. Deng and E. Barkai, Phys. Rev. E **79**, 011112 (2009).